

## Dissociative Ionization of Methylated Hydrazines

30 January 1995

Prepared by

B. B. BRADY and J. A. SYAGE  
Mechanics and Materials Technology Center  
Technology Operations

Prepared for

SPACE AND MISSILE SYSTEMS CENTER  
AIR FORCE MATERIEL COMMAND  
2430 E. El Segundo Boulevard  
Los Angeles Air Force Base, CA 90245

Space Technology Applications

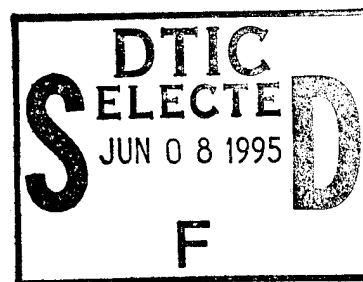
19950607 018



**THE AEROSPACE  
CORPORATION**  
El Segundo, California

APPROVED FOR PUBLIC RELEASE;  
DISTRIBUTION UNLIMITED

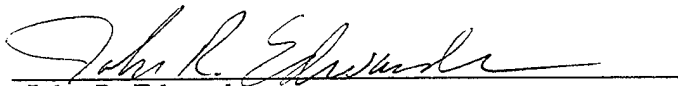
DTIC QUALITY INSPECTED 5



This report was submitted by The Aerospace Corporation, El Segundo, CA 90245-4691, under Contract No. F04701-93-C-0094 with the Space and Missile Systems Center, 2430 E. El Segundo Blvd., Los Angeles Air Force Base, CA 90245. It was reviewed and approved for The Aerospace Corporation by S. Feuerstein, Principal Director, Mechanics and Materials Technology Center, and T. Spiglanin, Systems Director, Environmental Programs.

This report has been reviewed by the Public Affairs Office (PAS) and is releasable to the National Technical Information Service (NTIS). At NTIS, it will be available to the general public, including foreign nationals.

This technical report has been reviewed and is approved for publication. Publication of this report does not constitute Air Force approval of the report's findings or conclusions. It is published only for the exchange and stimulation of ideas.

A handwritten signature in dark ink, appearing to read "John R. Edwards", is written over a horizontal line.

John R. Edwards  
Chief, Environmental Management Division  
Acquisition Civil Engineer  
Space and Missile Systems Center

REPORT DOCUMENTATION PAGE			Form Approved OMB No. 0704-0188	
Public reporting burden for this collection of information is estimated to average 1 hour per response, including the time for reviewing instructions, searching existing data sources, gathering and maintaining the data needed, and completing and reviewing the collection of information. Send comments regarding this burden estimate or any other aspect of this collection of information, including suggestions for reducing this burden to Washington Headquarters Services, Directorate for Information Operations and Reports, 1215 Jefferson Davis Highway, Suite 1204, Arlington, VA 22202-4302, and to the Office of Management and Budget, Paperwork Reduction Project (0704-0188), Washington, DC 20503.				
1. AGENCY USE ONLY (Leave blank)		2. REPORT DATE 30 January 1995		3. REPORT TYPE AND DATES COVERED
4. TITLE AND SUBTITLE DISSOCIATIVE IONIZATION OF METHYLATED HYDRAZINES			5. FUNDING NUMBERS  F04701-93-C-0094	
6. AUTHOR(S) Brady, Brian B., and Syage, Jack A.				
7. PERFORMING ORGANIZATION NAME(S) AND ADDRESS(ES) The Aerospace Corporation Technology Operations El Segundo, CA 90245-4691			8. PERFORMING ORGANIZATION REPORT NUMBER  TR-94(4231)-7	
9. SPONSORING/MONITORING AGENCY NAME(S) AND ADDRESS(ES) Space and Missile Systems Center Air Force Materiel Command 2430 E. El Segundo Blvd. Los Angeles Air Force Base, CA 90245			10. SPONSORING/MONITORING AGENCY REPORT NUMBER  SMC-TR-95-18	
11. SUPPLEMENTARY NOTES				
12a. DISTRIBUTION/AVAILABILITY STATEMENT Approved for public release; distribution unlimited.			12b. DISTRIBUTION CODE	
13. ABSTRACT (Maximum 200 words)  The dissociation of methylated hydrazine ions is observed to undergo extensive fragmentation and rearrangement leading to many fragments that have the same nominal mass, but differ in chemical composition by an N versus CH <sub>2</sub> moiety. In earlier work, we measured absolute ionization cross sections for hydrazine and methylhydrazine (MMH) dissociative ionization using a high throughput time-of-flight mass spectrometer that had excellent detectability of high kinetic energy ions, but only moderate mass resolution (0.1 amu). Here we employ high resolution quadrupole detection (0.005 amu) to distinguish ion fragments of the same nominal mass for MMH and unsymmetrical dimethylhydrazine (UDMH). The ratios of these close lying fragment masses are measured for different electron impact energies and explained in terms of thermochemical thresholds and fragmentation mechanisms. The methyl groups account for complex reaction mechanisms. A high yield is observed for NH dissociation induced by a 1,2 sigmatropic hydride shift and for CH <sub>4</sub> dissociation formed by a 1,2 elimination. Ion yield vs. thermochemical threshold plots are compared to model equilibrium curves and allow an estimate of the energy deposited by electron impact ionization and an assessment of how dissociative ionization differs for ambient vs. jet-cooled hydrazines. Departures of ion yield from the equilibrium curve are used to identify fragmentation reactions that involve large activation energies or unusual mechanisms.				
14. SUBJECT TERMS Hydrazines, Mass spectrometry, Fragmentation patterns			15. NUMBER OF PAGES 24	
			16. PRICE CODE	
17. SECURITY CLASSIFICATION OF REPORT Unclassified	18. SECURITY CLASSIFICATION OF THIS PAGE Unclassified	19. SECURITY CLASSIFICATION OF ABSTRACT Unclassified	20. LIMITATION OF ABSTRACT	

## Contents

1. Introduction.....	1
2. Experimental.....	2
3. Results and Discussion .....	3
3.1. Monomethyl Hydrazine (MMH) .....	4
3.2. Unsymmetrical Dimethyl Hydrazine (UDMH) .....	4
3.3. Rearrangements and Mechanisms.....	5
3.4. Ion Yield vs. Thermochemical Thresholds .....	6
4. Summary.....	8
References.....	8

## Tables

1. Thermochemical thresholds and relative intensities for MMH ionization fragments of the same nominal mass. ....	10
2. Thermochemical thresholds and relative intensities for UDMH ionization fragments of the same nominal mass. ....	11

## Figures

1. Mass spectra of ambient temperature $N_2H_4$ , MMH, and UDMH at 70 eV. ....	13
2. Mass spectra of jet-cooled MMH at 170 eV recorded in a molecular beam time-of-flight mass spectrometer. ....	14
3. Mass spectra of MMH at sufficient resolution to resolve fragments of the same nominal unit mass. ....	15
4. Mass spectra of UDMH showing distribution of three possible fragment ions for the same nominal mass. ....	16
5. Ion yield versus thermochemical energies for $N_2H_4$ . ....	17
6. Ion yield versus thermochemical energies for MMH. ....	18
7. Ion yield versus thermochemical energies for UDMH. ....	19

Accession For	
NTIS   CRA&I	<input checked="" type="checkbox"/>
DTIC   TAB	<input type="checkbox"/>
Unannounced	<input type="checkbox"/>
Justification .....	
By .....	
Distribution /	
Availability Codes	
Dist	Avail and/or Special
A-1	

## 1. Introduction

The series of hydrazine molecules  $\text{H}_2\text{NNH}_2$ ,  $\text{H}_2\text{NNH}(\text{CH}_3)$  (monomethylhydrazine, MMH), and  $\text{H}_2\text{NN}(\text{CH}_3)_2$  (unsymmetrical dimethylhydrazine, UDMH) are extensively used as propellant fuels for rocket and satellite thrusters. The vast majority of launch vehicle weight is composed of fuel and associated tankage and structural hardware. Any savings in weight for these components brought about by small improvements in thrust efficiency can lead to considerable increase in payload capacity. Even marginal improvements in engine performance have enormous economic benefit, which explains current interest in the study of spectroscopy and energetics of hydrazines and other propellant molecules. We have embarked on a course of study to better understand the spectroscopy and photodynamics of hydrazines under collision-free conditions as well as the chemical reactivity under single-collision conditions.<sup>1,2</sup>

Although electron-molecule collisions are only minor events in rocket propulsion, there are several reasons for studying these processes; (1) the dissociation mechanisms of ions are easy to follow relative to neutrals and often provide valuable insight into the chemical dynamics of neutral radical-molecule collisions, (2) electron-impact (EI) ionization mass spectrometry is a prominent analytical tool for atmospheric monitoring and requires an accurate data base of cross sections and fragmentation patterns, and (3) EI dissociative ionization of molecules is a convenient source of a wide variety of ions that may be useful for further study by gas-phase or matrix isolation ion (or neutral) spectroscopy.

Electron-impact and photoionization measurements of hydrazines are very limited.<sup>1-10</sup> Recently, we reported a comprehensive study on EI dissociative ionization cross sections, fragment appearance potentials, and fragment kinetic energies as a function of electron energy for jet-cooled  $\text{NH}_3$ ,  $\text{N}_2\text{H}_4$ , and MMH.<sup>1,2</sup> Other than this work, we are not aware of any cross-section measurements (either total or partial) for any hydrazine molecule. Berkowitz measured PI thresholds for the formation of  $\text{N}_2\text{H}_3^+$ , and  $\text{N}_2\text{H}_2^+$  fragments from  $\text{N}_2\text{H}_4$ .<sup>3,4</sup> Foner and Hudson measured EI thresholds for  $\text{N}_2\text{H}_2^+$  formation.<sup>6</sup> Besides our work, no threshold measurements for MMH dissociative ionization are available other than a very early photoionization<sup>5</sup> and electron-impact<sup>7</sup> study limited to larger fragments. Our cross section and kinetic energy measurements were made using a high throughput time-of-flight (TOF) mass spectrometer that had a larger kinetic energy detection window, but only moderate resolution (about 0.10 amu).<sup>2</sup>

In this work we are concerned with distinguishing the many fragments of methylated hydrazine ionization that have the same nominal mass, but differ in chemical composition by an N versus  $\text{CH}_2$  moiety. We employ high resolution quadrupole detection (0.005 amu) for this purpose. We report the ratios of these close lying fragment masses for different electron impact energies and explain the results in terms of thermochemical thresholds and fragmentation mechanisms.

## 2. Experimental

Two different mass spectrometers were used to record the spectra reported here. Ambient temperature mass spectra were recorded in a chamber containing a high resolution quadrupole mass spectrometer and jet-cooled spectra were recorded in a supersonic molecular beam time-of-flight mass spectrometer.

The high resolution mass spectra were taken with an Extrel quadrupole mass spectrometer, with a model 12 high Q head. Mass spectra were recorded over the entire mass range for  $N_2H_2$  and MMH. Extra capacitance was added to the high Q head to extend the mass range for measuring UDMH ionization, however, this was insufficient for collecting UDMH ion masses 55–60. As this is the first report on this spectrometer, we provide some details here. The quadrupole chamber is pumped by a 500 liter/sec turbo pump to a background pressure of  $2 \times 10^{-8}$  torr. The sample is introduced via an external gas line; the gas line consists of a sample holder that can be cooled and evacuated with a mechanical pump, a needle valve, and a 1/8th inch O.D. tube to introduce the sample 1/2 inch from the ionizer. The gas line is constructed of glass and stainless steel. The  $N_2H_4$ , MMH, and UDMH were purified by freeze-pump-thaw cycles using liquid nitrogen or  $CHCl_3$ /dry ice baths. The sample was cooled in ice water for delivery to the chamber.

Ambient spectra were recorded using sample pressures  $< 10^{-6}$  Torr. The ionizer was run with 1.0 mA emission current and the electron energy was varied as shown in the figures. The ion energy through the quadrupole was 10 eV for low resolution spectra and 3–5 eV for high resolution spectra. The resolution and  $\Delta m$  settings were adjusted to obtain separation between the  $CH_2$  and N moieties while trying to maintain a uniform mass detection efficiency. The electron multiplier was operated at 2.5–3.0 kV depending on the signal level. The multiplier anode current was sent to a current amplifier at  $1 \times 10^7$  V/A sensitivity and 30–100 ms time constant. Spectra were acquired by computer using an 8 bit DAC to sweep the masses and an 8 bit ADC to record the signal.

The molecular beam time-of-flight mass spectrometer has been described before.<sup>2,11</sup> A pulsed free jet expansion is skimmed to form a collimated molecular beam, which enters a high vacuum detection chamber (base pressure of  $2 \times 10^{-8}$  Torr rising to  $2 - 3 \times 10^{-7}$  during gas pulse operation). The molecular beam pulse is crossed by an electron beam pulse in a field free region between two grids. A voltage pulse is applied to one grid to extract ions out of this region into a second acceleration region involving a third grid. Ions exiting this region travel down a field-free drift tube and their arrival times are measured by a microchannel plate detector and digital oscilloscope.

The observed relative intensities of the fragment ions can deviate from their true values because of instrument effects. The collection efficiency of a quadrupole mass spectrometer has a mass dependence that depends on mode of operation. For ions injected parallel to the cavity axis, there are two simple governing relations that describe this dependence. The maximum injection aperture is given by

$$a \simeq \frac{2}{3} r_0 \left[ \frac{\Delta m}{m} \right]^{1/2} \quad (1)$$

and the maximum transverse energy is given by

$$\epsilon_{t,max} = \frac{1}{2} m f^2 r_0^2 \frac{\Delta m}{m} \quad (2)$$

where  $r_0$  is cavity radius,  $f$  is the rf frequency,  $m$  is mass, and  $\Delta m$  is the peak width.<sup>12</sup> These simple equations predict that  $a$  depends on mass to a power of 0 or  $-1$  depending on whether recording spectra under conditions of constant resolution  $\Delta m/m$  or constant peak width  $\Delta m$ , respectively. Similarly,  $\epsilon_{t,max}$  depends on mass to a power of 1 or 0 for the same conditions, respectively. The actual instrument mass dependence was measured by recording mass spectra of a calibrated mixture of He, Ne, and Ar.

It was not possible to measure directly the collection efficiency as a function of fragment ion kinetic energy in the quadrupole, other than to calculate it by Eq. (2). Fragment kinetic energies were measured in a previous study for jet-cooled  $N_2H_4$  and MMH in the molecular beam TOF mass spectrometer. The center-of-mass recoil energies for ionization generally range from 0.3–0.6 eV for  $N_2H_4$  and 0.2–0.5 eV for MMH and are relatively invariant over a range of 70–170 eV ionization energies.<sup>2</sup> The kinetic energies for UDMH ion fragmentation were not measured, but are expected to be less than for MMH and hydrazine due to the larger density of states for UDMH. Based on calculated  $\epsilon_{t,max}$ , the relative intensities in the high resolution mass spectra reported here are significantly affected by fragment kinetic energy, whereas the low resolution mass spectra are minimally affected by fragment kinetic energy.

The hydrazines are stored in a refrigerator. Samples are prepared in a hood by pipetting about 5 ml of hydrazine into a bubbler and then attaching valves to the bubbler ports. The sample is then transported to the apparatus and connected to polyflow delivery lines. Samples are purified by freeze-thaw cycles. We dispose of residual hydrazine in the bubbler by pouring it into a 1 gal plastic bottle filled about halfway with a calcium hypochlorite solution. The hypochlorite neutralizes the hydrazine and the large volume dissipates the heat release. The bubbler is flushed out a couple of times with hypochlorite solution and then water.

### 3. Results and Discussion

Low resolution EI ionization mass spectra of ambient temperature  $N_2H_4$ , MMH, and UDMH are given in Fig. 1. For comparison, a jet-cooled MMH EI mass spectrum is presented in Fig. 2. The ambient and jet-cooled MMH mass spectra are qualitatively different; the latter showing less apparent fragmentation. The difference between ambient and jet-cooled  $N_2H_4$  mass spectra (not shown here) was less noticeable. We did not record any jet-cooled UDMH mass spectra. Large differences in the ionization/fragmentation pattern for jet-cooled versus ambient temperature molecules have been observed before and indicate that the thermal energy content of molecules can contribute greatly to ion fragmentation efficiency.<sup>13–15</sup> We will return to this point later when we compare ion fragment yield to fragment equilibrium curves for different assumed internal ion energies.

The focus of this work is to resolve the relative intensities of fragments from MMH and UDMH ionization that have the same nominal mass. Examples of high resolution quadrupole mass spectra that resolve the fragment distributions are given in Figs. 3 and 4.

The full results are summarized in Tables 1 and 2. These results are described below. We compare fragment ions of the same mass for convenience and do not imply that there is a direct competition among these masses.

### 3.1. Monomethyl Hydrazine (MMH)

*Ion fragment masses 12–18:* These ions are accounted for by the structures  $\text{NH}_n^+$  and  $\text{CH}_n^+$ . Masses 17 and 18 are explained by fragments  $\text{NH}_3^+$  and  $\text{NH}_4^+$ . A distinct crossover develops in which the ion signals for masses 12–15 arise almost entirely from fragments  $\text{CH}_m^+$ ,  $m = 0–3$ . Mass 16 is due primarily to  $\text{NH}_2^+$ , even though  $\text{CH}_4^+$  has a much lower thermochemical threshold (Table 1). Though not obvious in the ambient spectrum in Fig. 1, a drop in intensity occurs for mass 16 relative to mass 15 in the jet-cooled mass spectrum in Fig. 2 that is consistent with two monotonically increasing series of ion signals corresponding to  $\text{NH}_n^+$  ( $n = 2–4$ , mass 16–18) and  $\text{CH}_n^+$  ( $n = 0–3$ , mass 12–15). Except for mass 16, the above fragment distributions conform to predictions based on thermochemical thresholds.

*Ion fragment masses 28–31:* This series of ions has contributions from  $\text{CNH}_n^+$  ( $n = 2–5$ ) and  $\text{N}_2\text{H}_n^+$  ( $n = 0–3$ ). Calculated thermochemical thresholds and relative intensities are compiled in Table 1. The  $\text{N}_2\text{H}_n^+$  series becomes increasingly more stable relative to the  $\text{CNH}_n^+$  series as  $n$  increases except at 30 amu. Essentially no  $\text{N}_2^+$  is formed by MMH ionization in contrast to  $\text{N}_2\text{H}_4$  ionization reported earlier.<sup>2</sup> Instead, the stable structure  $\text{CH}\equiv\text{NH}^+$  accounts for the mass 28 signal (Fig. 3). Simple  $\text{CH}_3$  loss to give  $\text{N}_2\text{H}_3^+$  accounts for most of ion fragment mass 31 and is consistent with the absence of a signal at mass 32. The other mass 31 fragment  $\text{CH}_3\text{NH}_2^+$  is formed by a 1,2 hydride shift and N–N bond cleavage, in analogy to  $\text{NH}_3^+$  formation in  $\text{N}_2\text{H}_4$  ionization. A stable  $\text{CH}_2=\text{NH}_2^+$  ion can then form by hydrogen dissociation. This ion can alternatively be formed by direct  $\text{NH}_2$  dissociation, which has a very low thermochemical threshold, but probably a high activation energy owing to the strong 5.6 eV N–N bond energy (partial double bond) for the ground electronic state of the ion.<sup>2</sup> Masses 29 and 30 are interesting because the thermodynamically more stable fragments  $\text{CHNH}_2^+$  and  $\text{CH}_2\text{NH}_2^+$  predominate at low electron energy, but the fragments  $\text{N}_2\text{H}^+$  and  $\text{N}_2\text{H}_2^+$  increase significantly in intensity at higher electron energy (Table 1). The appearance of  $\text{N}_2\text{H}^+$  and  $\text{N}_2\text{H}_2^+$  is explainable by a rearrangement and  $\text{CH}_4$  elimination mechanism similar to that which leads to  $\text{H}_2$  elimination in  $\text{N}_2\text{H}_4$ .<sup>2</sup>

### 3.2. Unsymmetrical Dimethyl Hydrazine (UDMH)

*Ion fragment masses 12–18:* The ion fragment distributions for these masses are similar to that observed for MMH in that masses 14 and 15 are due to  $\text{CH}_2^+$  and  $\text{CH}_3^+$  and masses 17 and 18 are due to  $\text{NH}_3^+$  and  $\text{NH}_4^+$ . These results correlate to the lowest thermochemical thresholds (Table 2). Unlike MMH, however, mass 16 contains a significant contribution from  $\text{CH}_4^+$ . Apparently, production of  $\text{CH}_4^+$  is facilitated in UDMH by the close proximity of H atoms about the two geminal methyl groups.

*Ion fragment masses 28–32:* Three series of masses are possible for UDMH;  $\text{N}_2\text{H}_n^+$  ( $n = 0–4$ ),  $\text{CNH}_n^+$  ( $n = 2–6$ ), and  $\text{C}_2\text{H}_n^+$  ( $n = 4–8$ ). No  $\text{N}_2^+$  was observed at any excitation energy, which agrees with the results for MMH. All three possible masses were observed for mass 29. For masses 31 and 32 the fragment with the highest thermochemical threshold,  $\text{N}_2\text{H}_3^+$  and  $\text{CH}_3\text{NH}_3^+$ , respectively, gave the strongest signal.



*Ion fragment masses 42-45:* The fragment ion distributions for these masses do not show a strong correlation with thermochemical threshold. The most stable products are not necessarily formed in greatest yield because they can involve large barriers (e.g., excited electronic state excitation), particularly for the common case of multiple dissociations and bond rearrangement. Still, it is surprising that the simple  $\text{CH}_3$  loss channel to produce the mass 45 fragment ion is very weak considering that the corresponding dissociation in MMH to form  $\text{N}_2\text{H}_3^+$  is so strong (Table 1).

### 3.3. Rearrangements and Mechanisms

Although we have compared the yields of ions of the same nominal mass for convenience, it is worth noting that they rarely compete with one another, but rather with other reactions leading to different ion masses. For example, the yield of the mass 15 channel  $\text{CH}_3^+ + \text{N}_2\text{H}_3$  for MMH ionization is affected more by the lower energy charge transfer channel  $\text{CH}_3 + \text{N}_2\text{H}_3^+$  than it is by  $\text{NH}^+$  production whose yield is similarly affected by the competing charge transfer channel  $\text{NH} + \text{CH}_2\text{NH}_3^+$ .

We have learned from our earlier work on  $\text{N}_2\text{H}_4$  and MMH that there is a large variety of competing reaction mechanisms for ion dissociation of hydrazines.<sup>2</sup> For MMH we observed, in addition to single-bond and sequential-bond dissociation, reactions resulting from rearrangements and eliminations. We will use this base of information to interpret the new observations reported here for MMH and UDMH. The results in Tables 1 and 2 show clear evidence of simple bond dissociation of neutral fragments H,  $\text{CH}_3$ , and  $\text{NH}_2$ . We are more interested here in discussing the evidence for reaction mechanisms due to rearrangements and eliminations.

*1,2 Sigmatropic shift:* An important mechanism for hydrazine ions is a hydride shift followed by cleavage of the N-N bond, i.e.,



where  $\text{R}_1\text{R}_2$  is either H,H ( $\text{N}_2\text{H}_4$ ), H, $\text{CH}_3$  (MMH) or  $\text{CH}_3,\text{CH}_3$  (UDMH). This mechanism was proposed to explain the large yield of  $\text{NH}_3^+$  formed by  $\text{N}_2\text{H}_4$  ionization.<sup>2,16</sup> The hydride shift leads to a reduction in the N-N bond energy (from about 5.6 eV to about 3.2 eV) and an increase in the N-H bond energy (from about 2.8 eV to  $\geq 3.5$  eV). The hydride shift complex  $\text{HN}-\text{NHR}_1\text{R}_2^+$  is calculated to lie 1.2 eV above the  $[\text{H}_2\text{N}-\text{NR}_2\text{R}_2]^+$  structure,<sup>17</sup> however, this barrier is easily surmounted judging by the abundance of  $\text{NH}_3^+$  formed by  $\text{N}_2\text{H}_4$  ionization. The 1,2 hydride shift should be facilitated by methylation because it lowers the ionization potential of nitrogen-based molecular orbitals at the site of substitution due to charge delocalization. Indeed the UDMH results show that loss of NH is the dominant reaction pathway at all energies studied (Fig. 1, Table 2).

*Elimination reactions:* From previous appearance potential measurements it was determined that concerted elimination of  $\text{CH}_4$  occurs with relative ease following MMH ionization.<sup>2</sup> However, it was not possible to distinguish at the time between a 1,1 and a 1,2 elimination. The latter mechanism was favored because it produces a  $\text{HN}=\text{NH}^+$  fragment ion that is about 0.2 eV lower energy than the alternative  $\text{N}=\text{NH}_2^+$  ion.<sup>18</sup> The UDMH results summarized in Table 2 allow us to rule out the 1,1 elimination in favor of the 1,2 elimination for the following two reasons: (1) geminal dimethyl substitution in UDMH pro-

hibits 1,1 elimination of  $\text{CH}_4$ , yet  $\text{CH}_4$  loss occurs to relatively high yield indicating a 1,2 elimination, and (2) 1,1 elimination to give  $\text{N}_2\text{H}_2^+ + \text{C}_2\text{H}_6$  is a negligible reaction as is the formation of any  $\text{C}_2\text{H}_n^+$  fragment ion. These observations explain why  $\text{HN}=\text{NH}^+$  is formed in high yield for MMH ionization, but is absent for UDMH ionization.

**$\text{NH}_4^+$  formation:** The thermochemical threshold for producing  $\text{NH}_4^+$  is very low for all three hydrazine molecules considered here. As discussed in our earlier work on jet-cooled hydrazines, the yield of this  $\text{NH}_4^+$  is considerably greater for MMH ionization than for  $\text{N}_2\text{H}_4$  ionization, which we attributed to the greater availability of hydrogen atoms in a rearrangement reaction for methyl substitution.<sup>2</sup> This observation is less apparent in the ambient temperature mass spectra in Fig. 1; however, these spectra do show that  $\text{NH}_4^+$  is formed in much greater yield for ionization of UDMH and MMH than for  $\text{N}_2\text{H}_4$ . While it is possible that  $\text{NH}_4^+$  can form by ion-molecule reactions in an ambient gas quadrupole mass spectrometer arrangement, we operated at pressures well below the point of concern. Furthermore, bimolecular product ions are very unlikely to occur in a pulsed molecular beam time-of-flight mass spectrometer where the original observation of  $\text{NH}_4^+$  for MMH was made.<sup>2,16b</sup>

### 3.4. Ion Yield vs. Thermochemical Threshold

Fragment ion yields are plotted versus thermochemical thresholds  $\Delta H$  in Figs. 5–7. These results show the expected trend of declining yield with increasing  $\Delta H$ . However, it is also evident that large deviations from this trend are observed. If all products were formed at equilibrium, then one might expect fragment yields  $I_i$  that vary smoothly and exponentially with  $\Delta H$  according to a simple equilibrium Boltzmann equation, such as

$$\frac{I_i}{\sum_i I_i} = A \exp \{-(\Delta H - E_{ip})/kT\} \quad (3)$$

where  $E_{ip}$  is the adiabatic ionization potential.<sup>1</sup> A thermal Boltzmann equation is not rigorously correct because the ions formed are not thermal, but have energy distributions determined by electronic state excitation and vibrational excitation determined by Franck-Condon factors for ionization. Though intramolecular energy redistribution occurs, there are no collisions to thermalize the energy. Still one can approximate  $I_i$  as a function of energy content  $E_x$  in the ion as

$$E_x = C_v T \sim \frac{m}{2} kT \quad (4)$$

where  $m$  represents the number of effective degrees of freedom in the parent ion.

It is useful to compare the measured ion yields  $I_i$  to Eqs. (3) and (4). The comparison is only qualitative because of the simplicity of this model and the uncertainties in measuring  $I_i$  described earlier (e.g., instrument effects, kinetic energy discrimination effects, difficulty in quantitatively measuring close lying fragments of the same nominal mass, etc.). Otherwise, deviations in ion yield from equilibrium can occur for a number of reasons, including; (1) product ions may further decompose (sequential fragmentation), (2) high activation energy, (3) state-specific dissociation or, more likely, direct dissociation from repulsive electronic states, (4) complicated reaction mechanism (e.g., extensive rearrangement or a restricted

phase space). In the following, we explore how well the  $I_i$  vs  $\Delta H$  plots correlate to the energy content of the ionized molecule.

Calculated equilibrium curves according to Eqs. (3) and (4) are plotted in Figs. 5–7. Because the fragments are formed in very non-equilibrium distributions, it is not reasonable to apply a fit to all the data. Instead, we plot calculated curves so as to approximately bracket the upper limit for ion yields. The general correlation of the experimental data to the Boltzmann relationship indicates that the parent ions are formed with considerable energy at 70 eV excitation. In Fig. 5, we obtain a value of  $kT \sim 2E_x/m \sim 3.5$  eV for both ambient and jet-cooled  $N_2H_4^+$ .

To determine total ion internal energy  $E_x$ , we need to estimate  $m$  in Eq. (4). In the high temperature limit, where  $kT$  is much greater than the highest frequency vibrations, one has  $m = 3n - 6$  ( $n$  is the number of atoms in the molecule and we exclude translations and rotations because they are not significantly excited by EI). Using Eq. (4) we obtain an internal ion energy for  $N_2H_4^+$  of  $E_x = 21$  eV. A similar analysis for methylated hydrazines in Figs. 6 and 7 yields 31.5 and 23.6 eV for ambient and jet-cooled MMH, respectively, and 45 eV for ambient UDMH. These values seem too large, especially for MMH and UDMH. From a previous analysis of hydrazine molecular orbitals, it was determined that there are several ion electronic states between 5 and 20 eV above the ion ground state. However, the next higher single-electron ionization state occurs at about 400 eV involving a core 1s nitrogen electron.<sup>2</sup> Hence, ion energies should not exceed 20 eV for 70 eV EI excitation. This assumes that the probability of exciting doubly excited states by a single ionizing electron is low.

If ionization/excitation involves excited electronic states rather than purely vibrational excitation, then the high temperature limit may not be valid. It is difficult to know the number of effective degrees of freedom  $m$  in the ion. If we use published values of  $C_p$  for neutral room temperature gases (11.8, 17.0, 14.4 cal mol<sup>-1</sup> deg<sup>-1</sup> for  $N_2H_4$ , MMH, UDMH, respectively)<sup>19</sup> and the easily derivable relation  $m = (C_p - k)/k$ , one then obtains from Eq. (4) ion energies of 17.5 eV (ambient and jet-cooled  $N_2H_4$ ), 22.5 and 16.9 eV (ambient and jet-cooled MMH, respectively), and 18.6 eV (ambient UDMH). These values are consistent with the known electronic state properties of the hydrazine ions.

The above analysis, though qualitative, provides an estimate of internal ion excitation, indicates that the high temperature limit does not prevail, and that excited electronic state energy is the dominant mechanism of ion excitation. The observed non-equilibrium distribution of ion fragments is consistent with excited electronic state excitations which have different bond energies and dissociative limits. In particular, proton dissociation for all three hydrazines appears to occur in enhanced yield relative to other fragments with similar values of  $\Delta H$  and may represent a product occurring by direction dissociation from a repulsive excited electronic state.

Finally, we comment on the differences observed for dissociative ionization of ambient temperature versus jet-cooled molecules. For simplicity we assume that the ambient sample is at 300 K and the jet-cooled sample is at 0 K. Using the  $C_p$  values above, the thermal energy content of the ambient molecules relative to 0 K is 0.11 eV and 0.17 eV for  $N_2H_4$  and MMH, respectively. These energies are small relative to the energy deposited by ionization. This interpretation explains the similar fragmentation behavior and internal energy for ambient

and jet-cooled  $\text{N}_2\text{H}_4$ , but is inconsistent with the noticeably different results for ambient and jet-cooled MMH. We hesitate to attach too much significance to a comparison of dissociative ionization results for ambient and jet-cooled molecules because the measurements were made using mass spectrometers of very different characteristics.

#### 4. Summary

The dissociation of methylated hydrazine ions is observed to undergo extensive fragmentation and rearrangement leading to many fragments that have the same nominal mass, but differ in chemical composition by an N versus  $\text{CH}_2$  moiety. In earlier work, we measured absolute ionization cross sections for hydrazine and methylhydrazine (MMH) dissociative ionization using a high throughput time-of-flight mass spectrometer that had excellent detectability of high kinetic energy ions, but only moderate mass resolution (0.1 amu). Here we employ high resolution quadrupole detection (0.005 amu) to distinguish ion fragments of the same nominal mass for MMH and unsymmetrical dimethylhydrazine (UDMH). The ratios of these close lying fragment masses are measured for different electron impact energies and explained in terms of thermochemical thresholds and fragmentation mechanisms. The methyl groups account for complex reaction mechanisms. A high yield is observed for NH dissociation induced by a 1,2 sigmatropic hydride shift and for  $\text{CH}_4$  dissociation formed by a 1,2 elimination. Ion yield vs. thermochemical threshold plots are compared to model equilibrium curves and allow an estimate of the energy deposited by electron impact ionization and an assessment of how dissociative ionization differs for ambient vs. jet-cooled hydrazines. Departures of ion yield from the equilibrium curve are used to identify fragmentation reactions that involve large activation energies or unusual mechanisms.

#### References

1. Syage, J. A.; Cohen, R. B.; Steadman, J. *J. Chem. Phys.* **1992**, *97*, 6072.
2. Syage, J. A. *J. Chem. Phys.* **1992**, *97*, 6085.
3. Ruscic, B.; Berkowitz, J. *J. Chem. Phys.* **1991**, *95*, 4378.
4. Gibson, S. T.; Greene, J. P.; Berkowitz, J. *J. Chem. Phys.* **1985**, *83*, 4319.
5. Akopyan, M. E.; Vilesov, F. I. *Engl. trans. Kinet. Catal* **1962**, *4*, 32; Akopyan, M. E.; Vilesov, F. I.; Terenin, A. N. *Bull. Acad. Sci. USSR Phys. Ser.* **1963**, *27*, 1504.
6. Foner, S. N.; Hudson, R. L. *J. Chem. Phys.* **1978**, *68*, 3162.
7. Dibeler, V. H.; Franklin, J. L.; Reese, R. M. *J. Am. Chem. Soc.* **1959**, *81*, 68.
8. Osafune, K.; Katsumata, S.; Kimura, K. *Chem. Phys. Lett.* **1973**, *19*, 369.
9. Bodor, N.; Dewar, M. J. S.; Jennings, W. B.; Worley, S. D. *Tetrahedron*, **1970**, *26*, 4109; Nelsen, S. F.; Buschek, J. M. *J. Am. Chem. Soc.* **1974**, *96*, 2392.
10. Frost, D. C.; Lee, S. T.; McDowell, C. A.; Westwood, N. P. C. *J. Chem. Phys.* **1976**, *64*, 4719.
11. Syage, J. A. *Phys. Rev. A* **1992**, *46*, 5666; Syage, J. A. *J. Chem. Phys.* **1990**, *92*,

- 1804; Syage, J. A.; Steadman, J. *Rev. Sci. Instrum.* **1990**, *61*, 1204.
12. Extrel operators manual, *Flange Mounted Mass Filter Assembly*, chap 6.
13. Syage, J. A.; Pollard, J. E.; Cohen, R. B. *Appl. Opt.* **1987**, *26*, 3516; Sass S.; Fisher, T. L. *Org. Mass Spectrom.* **1979**, *14*, 257.
14. Amirav, A. *Org. Mass Spectrom.* **1991**, *26*, 1; Amirav, A. *J. Phys. Chem.* **1990**, *94*, 5200.
15. Turecek, F. *Org. Mass Spectrom.* **1991**, *26*, 1074.
16. (a) The possibility of an  $\text{NH}_3$  impurity accounting for  $\text{NH}_3^+$  was ruled out by KE measurements of the ion. (b) Ion-molecule collisions were also discounted owing to the collisionless nature of the pulsed molecular beam and other experimental safeguards (Ref. 2).
17. Drewello, T.; Lebrilla, C. B.; Schwarz, H.; Stahl, D. *Int J. Mass Spectrom. Ion Proc.* **1987**, *77*, R3.
18. Pople, J. A.; Curtiss, L. A. *J. Chem. Phys.* **1991**, *95*, 4385.
19. Wagman, D. D.; et al., *J. Phys. Chem. Ref. Data* **1982**, *11*, 2-1.
20. Lias, S. G.; Bartmess, J. E.; Liebman, J. F.; Holmes, J. L.; Levin, R. D.; Mallard, W. G. *J. Phys. Chem. Ref. Data* **1988**, *17*, 1.
21. Lias, S. G.; Liebman, J. F.; Levin, R. D. *J. Phys. Chem. Ref. Data* **1984**, *13*, 695.
22. McMillen, D. F.; Golden, D. M. *Ann. Rev. Phys. Chem.* **1982**, *33*, 493, and references therein.

TABLE 1. Thermochemical thresholds and relative intensities for MMH ionization fragments of the same nominal mass.

Mass	Fragment	$\Delta H$ (eV) <sup>a</sup>	Relative Intensity <sup>b</sup>			Ion Yield (70 eV) <sup>c</sup>	
			15 eV	25 eV	70 eV	amb	jet <sup>d</sup>
14.003	$N^+ CH_3NH_2 + H$	20.48	--	--	0		
14.016	$CH_2^+ N_2 + 2H_2$	13.38	--	--	100	3.6	2.1
15.011	$NH^+ CH_3NH_2$	16.18	0	--	20	1.6	0.7
15.023	$CH_3^+ + N_2 + H_2 + H$	12.62	100	--	80	6.3	2.9
16.019	$NH_2^+ + CH_2NH_2$	13.77	100	--	100	5.5	2.2
16.031	$CH_4^+ + N_2 + H_2$	10.78	0	--	0		
17.026	$NH_3^+ + CH_2NH$	10.09	100	--	100	6.2	3.8
17.039	$CH_5^+ + N_2 + H$	10.65	0	--	0		
18.034	$NH_4^+ + CHNH$	10.08	100	--	100	12.4	9.8
28.006	$N_2^+ + CH_4 + H_2$	13.83	10	10	10	1.5	1.8
28.019	$CHNH^+ + NH_3 + H$	10.61	90	90	90	12.9	15.9
29.014	$N_2H^+ + CH_4 + H$	11.24	60	60	80	3.5	6.1
29.026	$CHNH_2^+ + NH_3$	9.73	40	40	20	0.7	1.5
30.022	$N_2H_2^+ + CH_4$	10.18	10	20	25	1.4	1.4
30.034	$CH_2NH_2^+ + NH_2$	8.70	90	80	75	4.2	4.2
31.029	$N_2H_3^+ + CH_3$	10.54	60	80	90	6.0	11.4
31.042	$CH_2NH_3^+ + NH$	<11.64	40	20	10	0.7	1.3

<sup>a</sup> Values are relative to the neutral molecule and were first reported in Ref. 2 and determined using data from Refs. 2-4 and 20-22. Only the lowest energy fragmentation channel is shown for each mass. Higher energy channels are reported in Ref. 2. <sup>b</sup> Relative intensities for components of the same mass. Values are subject to KE discrimination effect as discussed in the text and are presented to show trends rather than absolute yields. Entries marked by dashes denote unmeasured data. <sup>c</sup> Ion yield as a percent of total ions. <sup>d</sup> The yields for different fragments of the same mass were determined using the ambient data in column 6. Analogous data for jet-cooled samples was not possible due to the limited resolution of our molecular beam TOF mass spectrometer.

TABLE 2. Thermochemical thresholds and relative intensities for UDMH ionization fragments of the same nominal mass.

Mass	Fragment	$\Delta H(\text{eV})^a$	Relative Intensity <sup>b</sup>		Ion Yield (70 eV) <sup>c</sup>
			17 eV	70 eV	
14.003	$\text{N}^+ + \text{CH}_3\text{CH}_2 + \text{NH}_3$	19.22	0	0	
14.016	$\text{CH}_2^+ + \text{CH}_4 + \text{N}_2 + \text{H}_2$	12.63	100	100	4.5
15.011	$\text{NH}^+ + \text{CH}_3\text{CH}_2\text{NH}_2$	16.25	0	0	
15.023	$\text{CH}_3^+ + \text{CH}_3 + \text{N}_2 + \text{H}_2$	12.84	100	100	14.7
16.019	$\text{NH}_2^+ + (\text{CH}_3)_2\text{N}$	13.66	10	60	1.4
16.031	$\text{CH}_4^+ + \text{CH}_4 + \text{N}_2$	10.03	90	40	0.9
17.026	$\text{NH}_3^+ + \text{CH}_3\text{CH}=\text{NH}$	8.81	100	100	1.8
17.039	$\text{CH}_5^+ + \text{CH}_3 + \text{N}_2$	9.92	0	0	
18.034	$\text{NH}_4^+ + \text{CH}_4 + \text{CN}$	9.33	100	100	18.5
18.047	$\text{CH}_6^+ + \text{CH}_2\text{N}_2$	13.18	0	0	
27.012	$\text{HCN}^+ + \text{CH}_4 + \text{NH}_3$	14.05	30 <sup>d</sup>	70	1.1
27.024	$\text{C}_2\text{H}_3^+ + \text{N}_2 + 2\text{H}_2 + \text{H}$	13.82	70 <sup>d</sup>	30	0.5
28.006	$\text{N}_2^+ + \text{C}_2\text{H}_6 + \text{H}_2$	13.76	0	0	
28.019	$\text{CHNH}^+ + \text{CH}_4 + \text{NH}_2$	10.03	100	100	11.8
28.031	$\text{C}_2\text{H}_4^+ + \text{N}_2 + 2\text{H}_2$	10.10	0	0	
29.014	$\text{N}_2\text{H}^+ + \text{C}_2\text{H}_6 + \text{H}$	11.17	50 <sup>d</sup>	60 <sup>d</sup>	1.2
29.026	$\text{CHNH}_2^+ + \text{CH}_3\text{NH}_2$	10.08	45 <sup>d</sup>	35 <sup>d</sup>	0.7
29.039	$\text{C}_2\text{H}_5^+ + \text{N}_2 + \text{H}_2 + \text{H}$	10.65	5 <sup>d</sup>	5 <sup>d</sup>	0.1
30.022	$\text{N}_2\text{H}_2^+ + \text{C}_2\text{H}_6$	10.10	0	0	
30.034	$\text{CH}_2\text{NH}_2^+ + \text{CH}_2\text{NH}_2$	8.41	100	100	5.7
30.047	$\text{C}_2\text{H}_6^+ + \text{N}_2 + \text{H}_2$	9.70	0	0	
31.029	$\text{N}_2\text{H}_3^+ + \text{C}_2\text{H}_5$	10.27	--	70	0.3
31.042	$\text{CH}_2\text{NH}_3^+ + \text{CHNH}_2$	9.15	--	30	0.2
31.055	$\text{C}_2\text{H}_7^+ + \text{N}_2 + \text{H}$	10.07	--	0	
32.037	$\text{N}_2\text{H}_4^+ + \text{C}_2\text{H}_4$	8.69	0	0	
32.050	$\text{CH}_3\text{NH}_3^+ + \text{CN} + \text{H}_2$	9.89	100	100	1.0
32.062	$\text{C}_2\text{H}_8^+ + \text{N}_2$	9.67	0	0	
42.022	$\text{CH}_2\text{N}_2^+ + \text{CH}_4 + \text{H}_2$	9.68	90	80	9.5
42.034	$\text{CH}_3\text{CNH}^+ + \text{NH}_3 + \text{H}$	9.28	10	20	2.4

43.029	$\text{CH}_3\text{N}_2^+ + \text{CH}_4 + \text{H}$	9.90	60	70	3.4
43.042	$\text{CH}_2=\text{CHNH}_2^+ + \text{NH}_3$	7.07	40	30	1.5
44.037	$\text{CH}_3\text{N}=\text{NH}^+ + \text{CH}_4$	9.03	30	50	1.4
44.050	$(\text{CH}_3)_2\text{N}^+ + \text{NH}_2$	7.68	70	50	1.4
45.045	$\text{CH}_3\text{N}_2\text{H}_2^+ + \text{CH}_3$	- -	10	10	0.6
45.058	$(\text{CH}_3)_2\text{NH}^+ + \text{NH}$	10.97	90	90	5.9

---

<sup>a</sup> Values are relative to the neutral molecule and were determined using data from Refs. 2-4 and 20-22. <sup>b</sup> Values are subject to KE discrimination effect as discussed in the text and are presented to show trends rather than absolute yields. Entries marked by dashes represent signals too weak to be meaningful. <sup>c</sup> Ion yield as a percent of total ions (excluding the undetected ions from 55-60 amu). <sup>d</sup> 25 eV ionization.



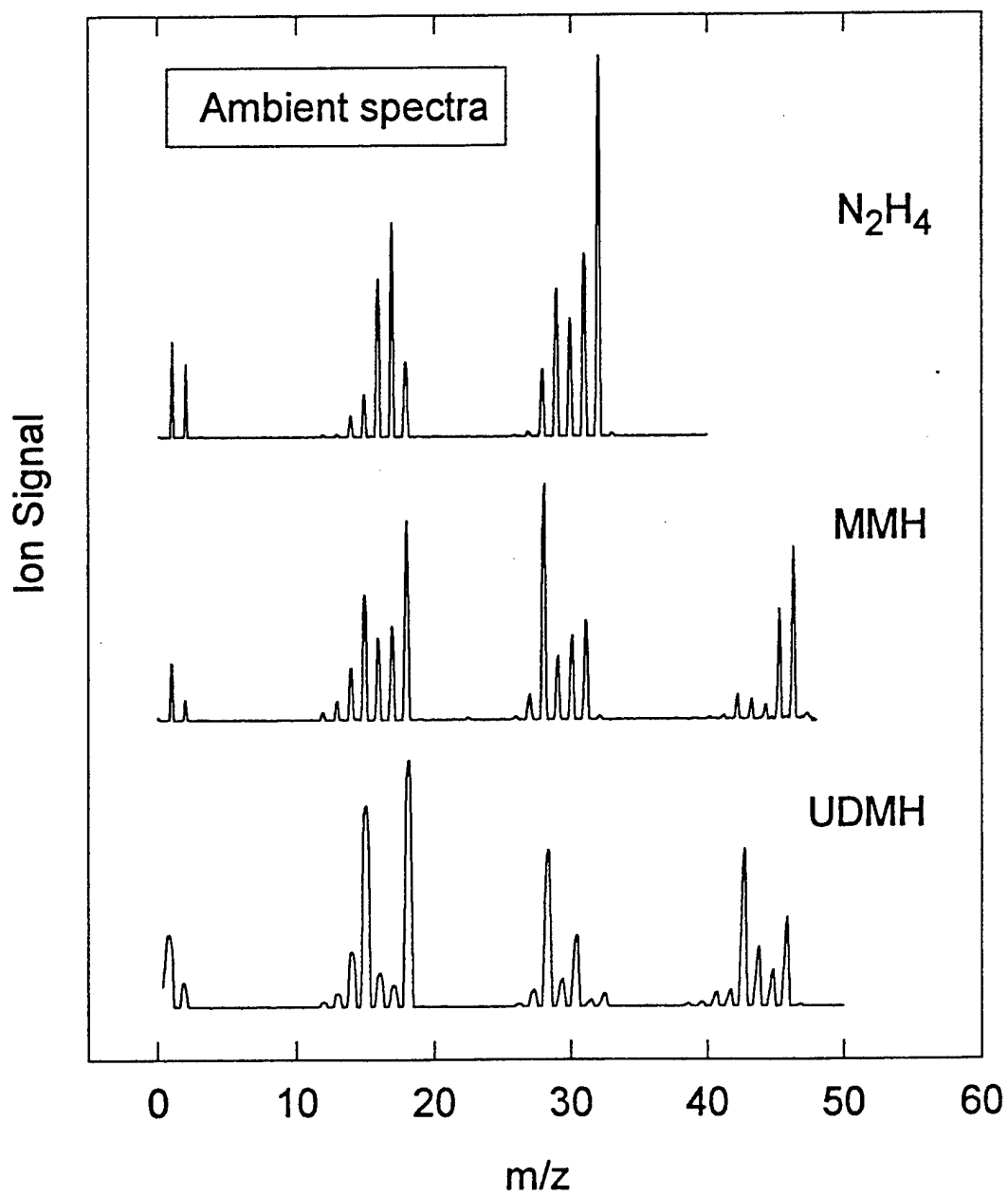


Figure 1. Mass spectra of ambient temperature N<sub>2</sub>H<sub>4</sub>, MMH, and UDMH at 70 eV. The parent and fragment ions of UDMH at 55–60 amu were outside the range of our spectrometer.

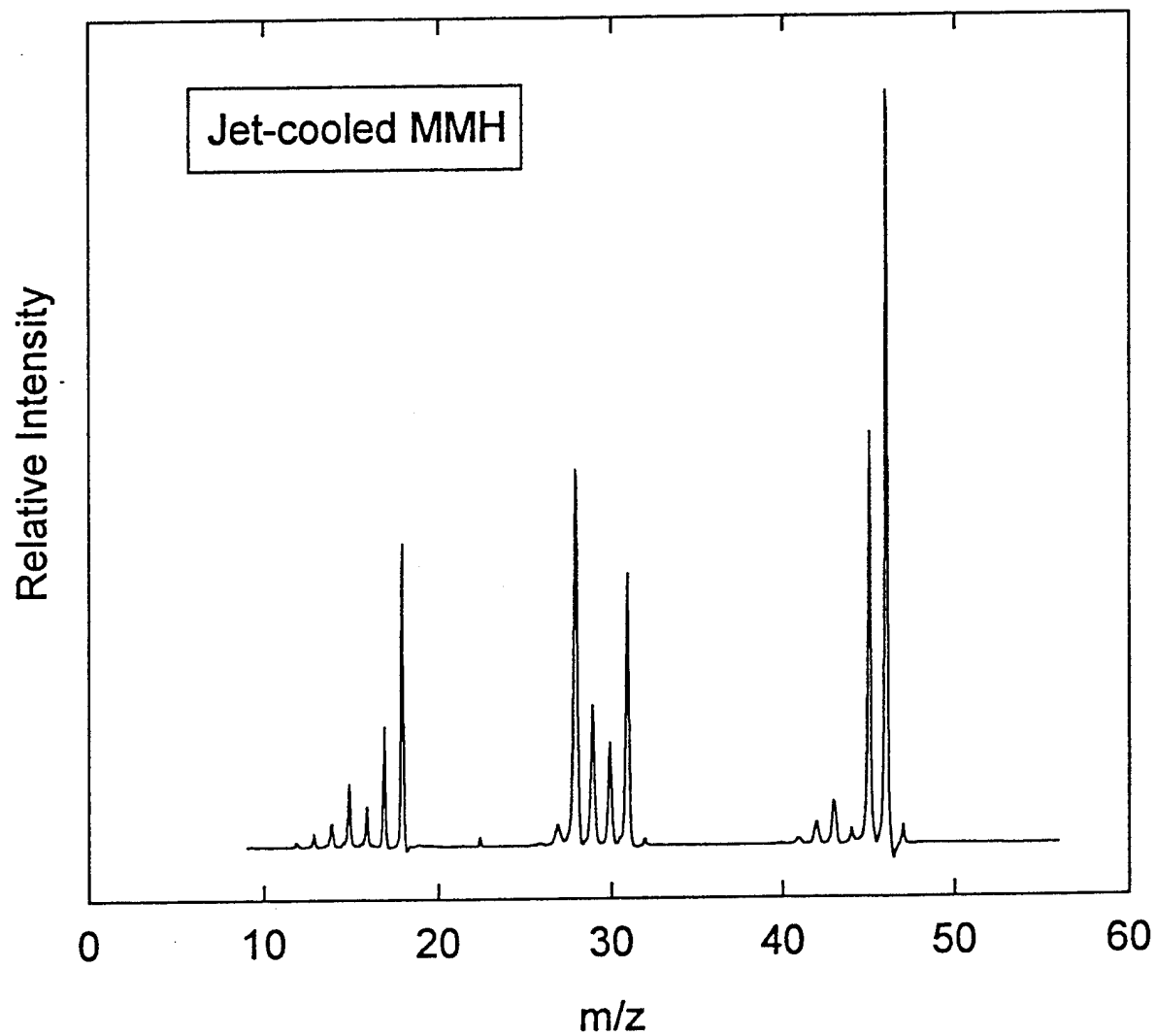


Figure 2. Mass spectra of jet-cooled MMH at 170 eV recorded in a molecular beam time-of-flight mass spectrometer. A 70 eV spectrum looks very similar.

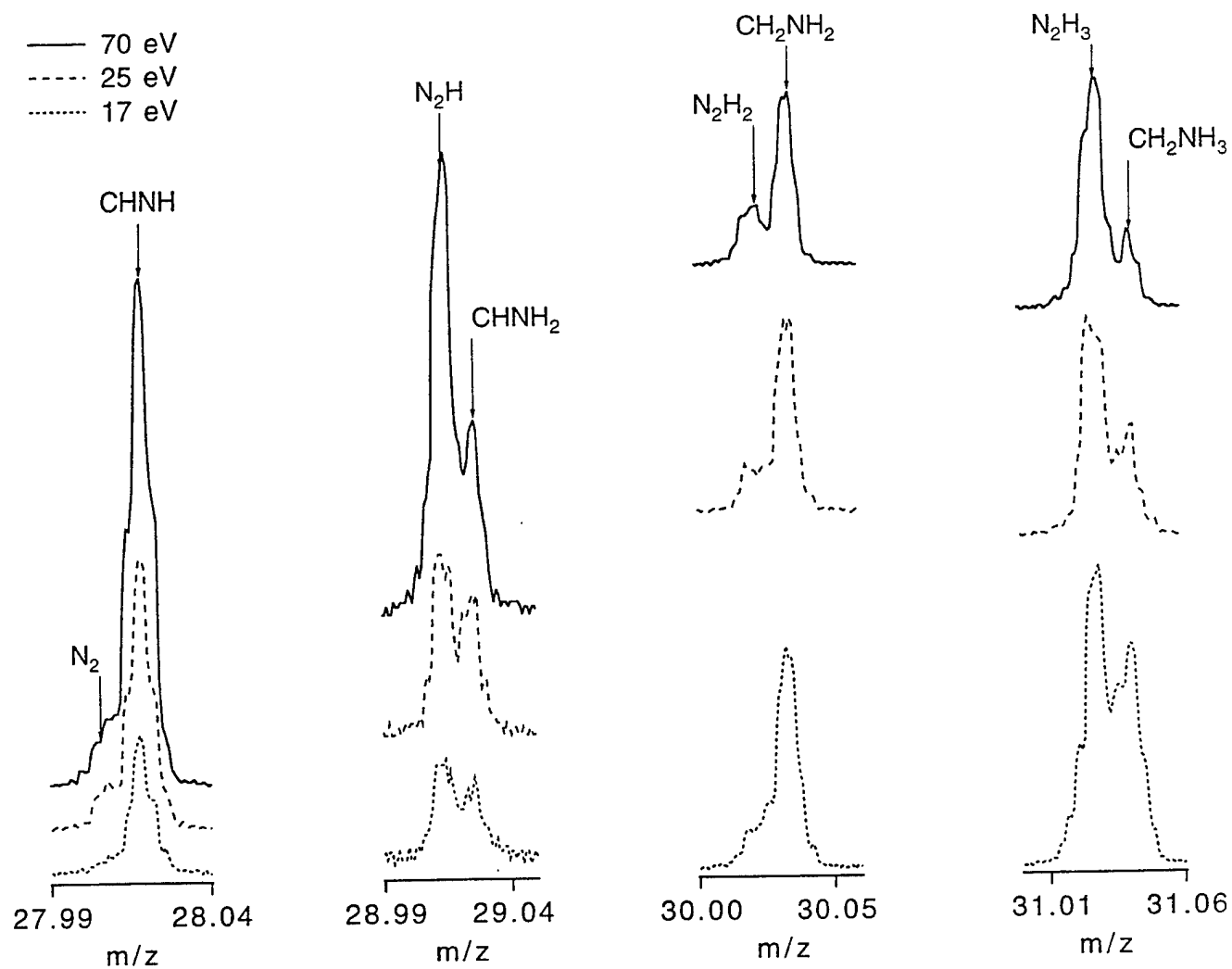


Figure 3. Mass spectra of MMH at sufficient resolution to resolve fragments of the same nominal unit mass. Spectra show variation of fragment relative yields with electron energy.

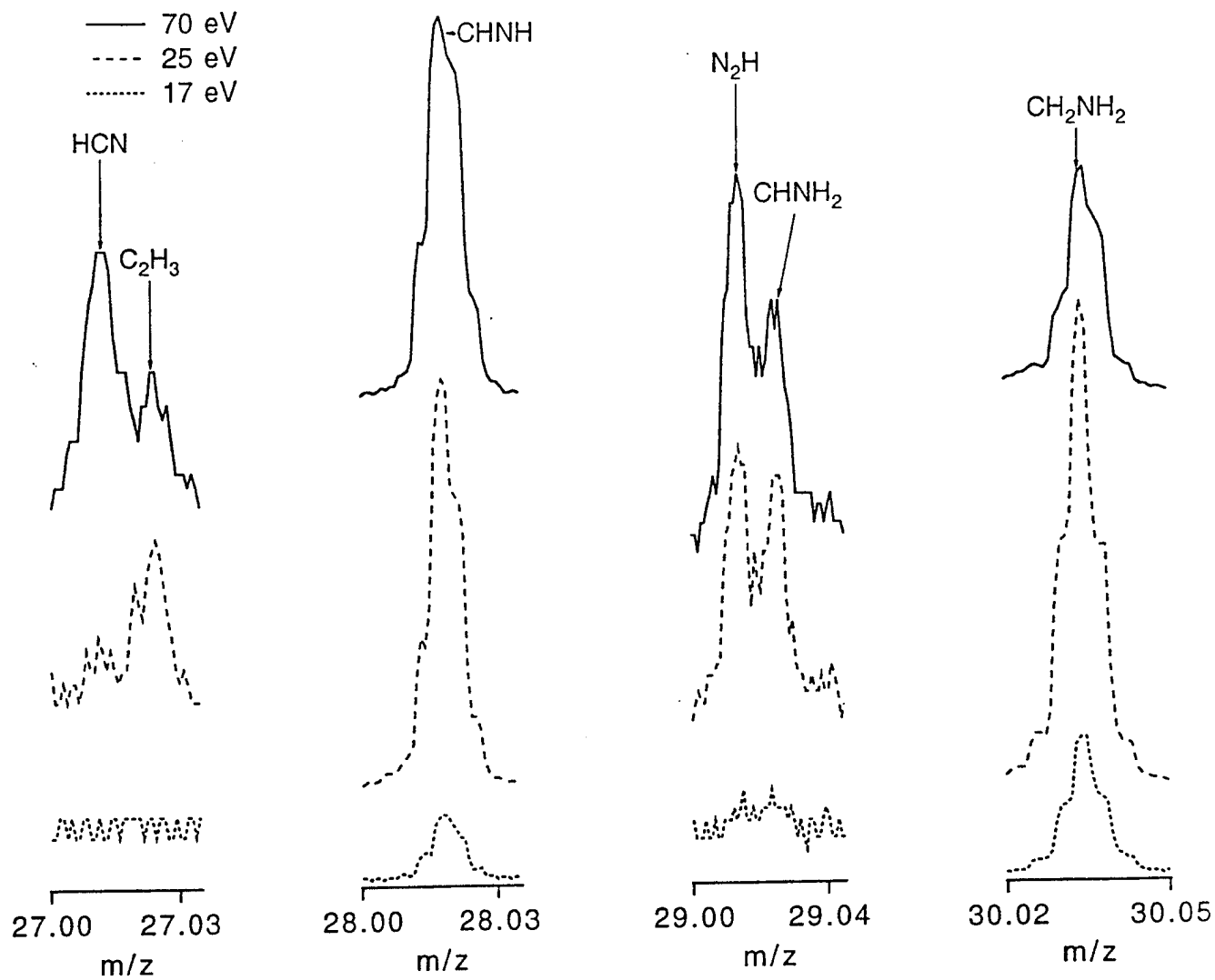


Figure 4. Mass spectra of UDMH showing distribution of three possible fragment ions for the same nominal mass.

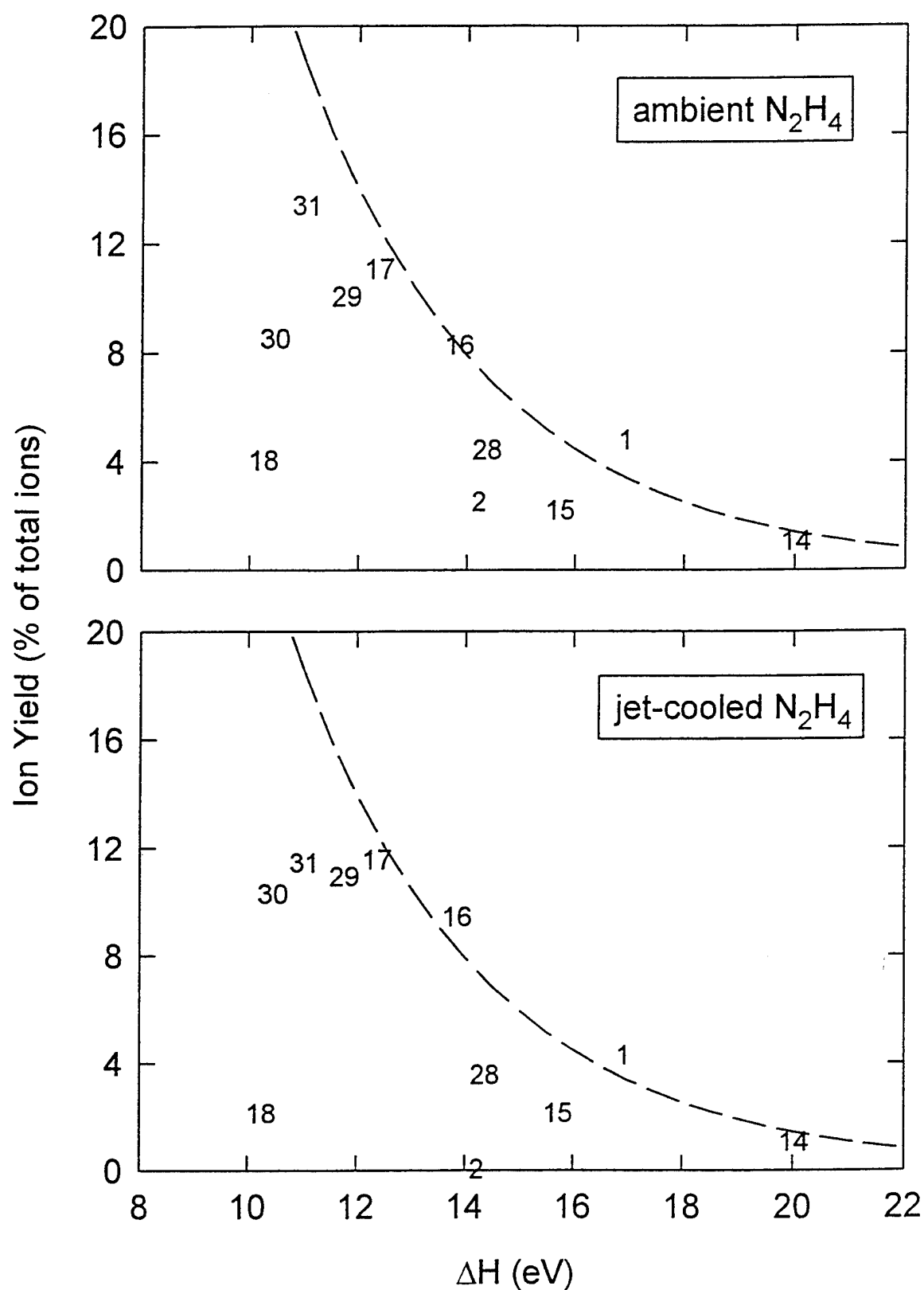


Figure 5. Ion yield versus thermochemical energies for  $N_2H_4$ . The numerical symbols represent the mass of the fragment. The calculated curve corresponds to Eq. (3) where  $A = 40$ ,  $2E_x/m = 3.5$  eV, and  $E_{IP} = 8.32$  eV for both the ambient and jet-cooled data. The parent ion has a yield of 29.5% and 33.5% for ambient and jet-cooled sample, respectively.

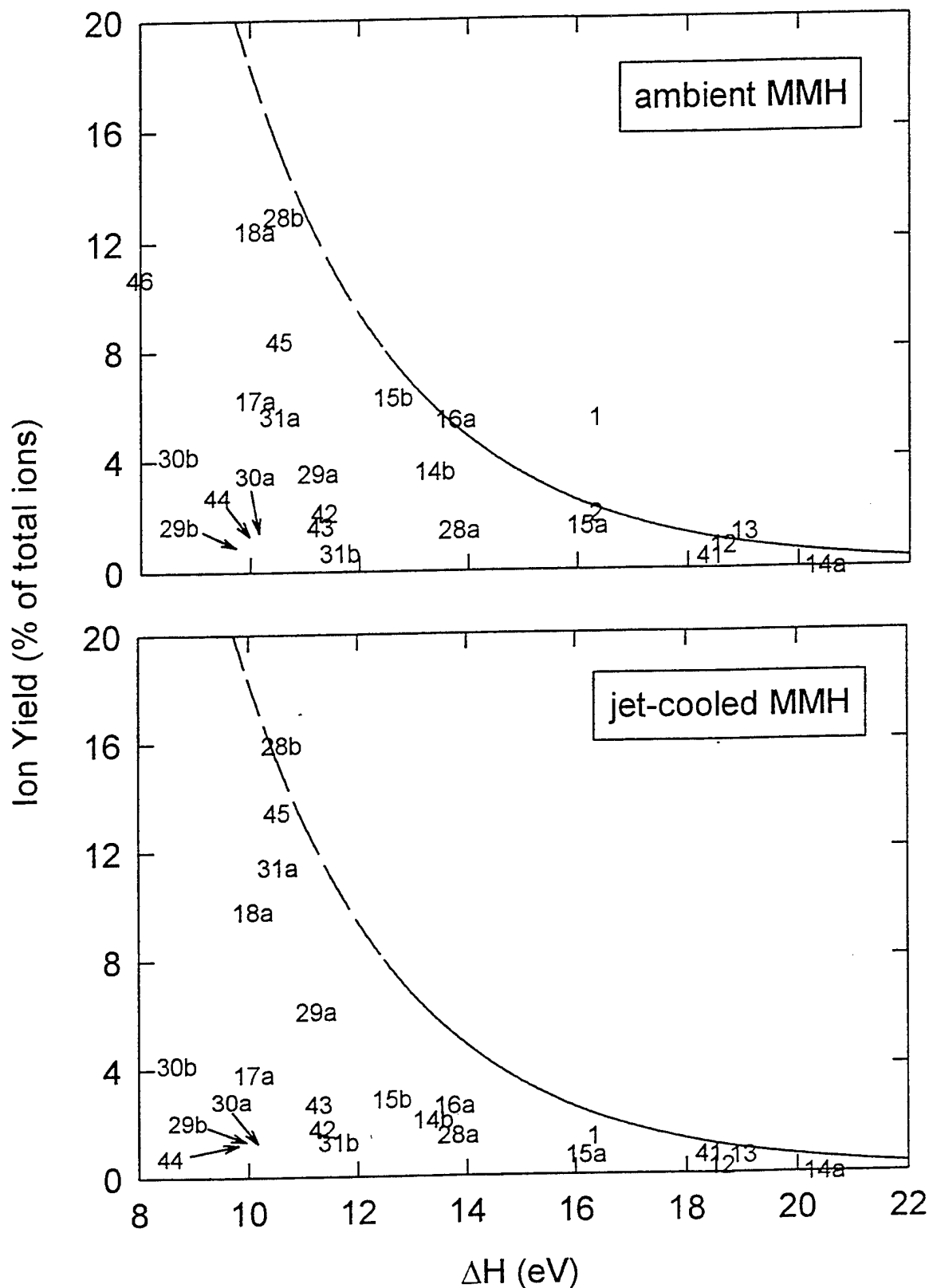


Figure 6. Ion yield versus thermochemical energies for MMH. The numerical symbols represent the mass of the fragment and the letter suffix distinguishes different fragments of the same nominal mass in ascending order by mass (cf. Table 1). The calculated curve corresponds to Eq. (3) where  $A = 35$  and  $2E_x/m = 3$  eV for ambient MMH and  $A = 50$  and  $2E_x/m = 2.25$  eV for jet-cooled MMH, and  $E_{IP} = 8.05$  eV. The ions 16b and 17b have zero yield and are not shown for clarity. The parent ion has a yield of 10.7% and 23.1% for ambient and jet-cooled sample, respectively.

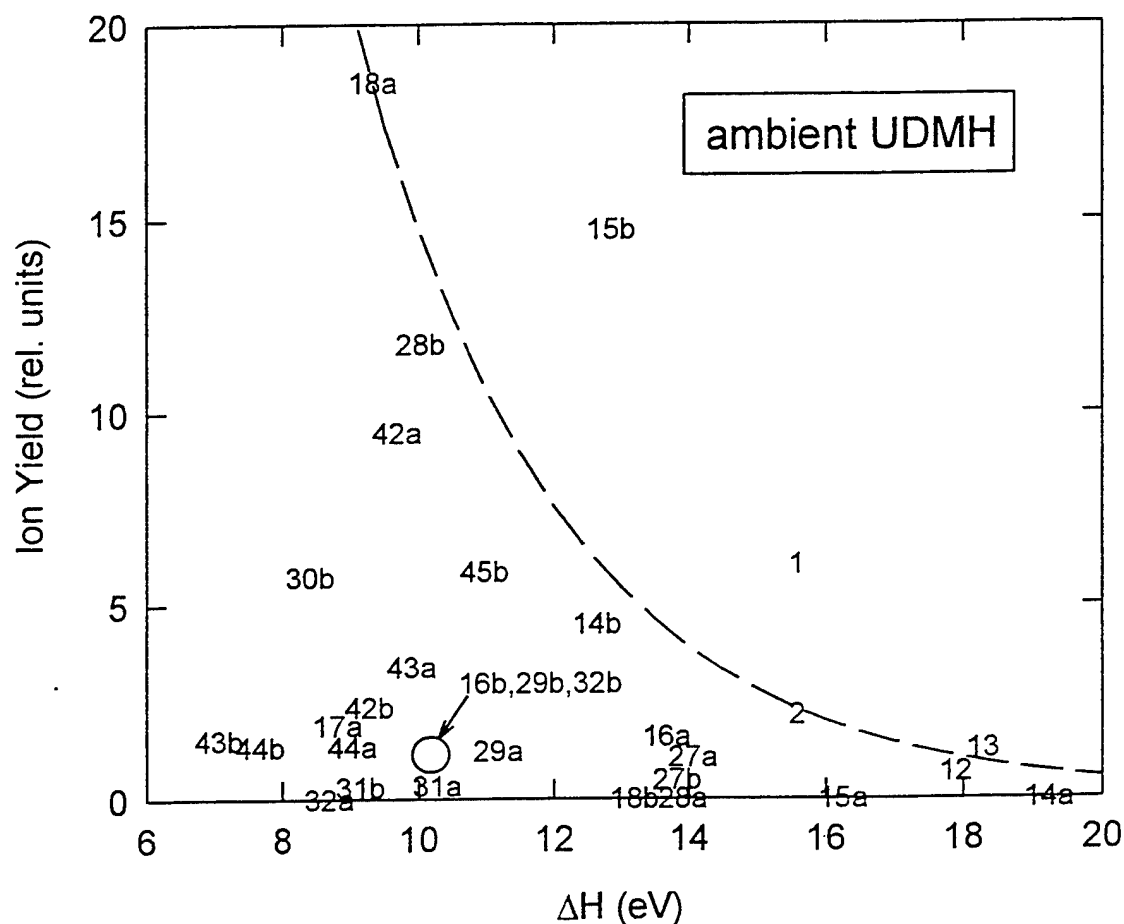


Figure 7. Ion yield versus thermochemical energies for UDMH. The numerical symbols represent the mass of the fragment and the letter suffix distinguishes different fragments of the same nominal mass in ascending order by mass (cf. Table 2). The calculated curve corresponds to Eq. (3) where  $A = 30$ ,  $2E_x/m = 3$  eV, and  $E_{IP} = 7.87$  eV. The overlapping symbols 17b, 28c, 29c, 30a, 30c, 31c, 32c at zero yield near 10 eV are not shown for clarity. The parent ion at mass 60 amu was not recorded.

## TECHNOLOGY OPERATIONS

The Aerospace Corporation functions as an "architect-engineer" for national security programs, specializing in advanced military space systems. The Corporation's Technology Operations supports the effective and timely development and operation of national security systems through scientific research and the application of advanced technology. Vital to the success of the Corporation is the technical staff's wide-ranging expertise and its ability to stay abreast of new technological developments and program support issues associated with rapidly evolving space systems. Contributing capabilities are provided by these individual Technology Centers:

**Electronics Technology Center:** Microelectronics, VLSI reliability, failure analysis, solid-state device physics, compound semiconductors, radiation effects, infrared and CCD detector devices, Micro-Electro-Mechanical Systems (MEMS), and data storage and display technologies; lasers and electro-optics, solid state laser design, micro-optics, optical communications, and fiber optic sensors; atomic frequency standards, applied laser spectroscopy, laser chemistry, atmospheric propagation and beam control, LIDAR/LADAR remote sensing; solar cell and array testing and evaluation, battery electrochemistry, battery testing and evaluation.

**Mechanics and Materials Technology Center:** Evaluation and characterization of new materials: metals, alloys, ceramics, polymers and their composites, and new forms of carbon; development and analysis of thin films and deposition techniques; nondestructive evaluation, component failure analysis and reliability; fracture mechanics and stress corrosion; development and evaluation of hardened components; analysis and evaluation of materials at cryogenic and elevated temperatures; launch vehicle and reentry fluid mechanics, heat transfer and flight dynamics; chemical and electric propulsion; spacecraft structural mechanics, spacecraft survivability and vulnerability assessment; contamination, thermal and structural control; high temperature thermomechanics, gas kinetics and radiation; lubrication and surface phenomena.

**Space and Environment Technology Center:** Magnetospheric, auroral and cosmic ray physics, wave-particle interactions, magnetospheric plasma waves; atmospheric and ionospheric physics, density and composition of the upper atmosphere, remote sensing using atmospheric radiation; solar physics, infrared astronomy, infrared signature analysis; effects of solar activity, magnetic storms and nuclear explosions on the earth's atmosphere, ionosphere and magnetosphere; effects of electromagnetic and particulate radiations on space systems; space instrumentation; propellant chemistry, chemical dynamics, environmental chemistry, trace detection; atmospheric chemical reactions, atmospheric optics, light scattering, state-specific chemical reactions and radiative signatures of missile plumes, and sensor out-of-field-of-view rejection.